Transport regimes in nitrogen-doped carbon nanotubes: Perfect order, semi-random, and random disorder cases

Hafid Khalfoun,[1,2] Aurélien Lherbier,[3] Philippe Lambin,[2] Luc Henrard,[2] and Jean-Christophe Charlier[3]

[1]*Université Hassiba Benbouali, Faculté des Sciences,*
Laboratoire de Physique Théorique et Physique des Matériaux (LPTPM), 02000 Chlef, Algéria

[2]*University of Namur, Carbon nanostructures research group and department of Physics, Rue de Bruxelles 61, 5000 Namur, Belgium*

[3]*Université catholique de Louvain, Institute of Condensed Matter and Nanosciences (IMCN),*
Chemin des étoiles 8, 1348 Louvain-la-Neuve, Belgium

The electronic structure and the transport properties of nitrogen-doped carbon nanotubes are investigated using a tight-binding model and a real-space Kubo-Greenwood approach, respectively. The transport regimes of various axial and helical doping configurations, from perfectly periodic to fully random disordered cases, are examined through the time dependence of the diffusivity. By varying the degree of disorder, a rich set of transient regimes is predicted going from persisting quasiballistic to momentarily localized regimes. A spectacular long-time ballistic regime is also observed for a specific semi-random disorder doping configuration owing to symmetry effects.

I. INTRODUCTION

Electronic transport in one dimensional (1D) systems is very sensitive to the presence and type of disorder. In particular, intrinsic defect impurities such as doping with substitutional foreign atoms induce usually strong resonant backscattering. Actually, whatever the strength of the disorder, all the electronic states are localized in disordered 1D systems in the thermodynamical limit according to the scaling theory of localization [1–5]. However, a broad variety of disorder exists, from the almost perfect ordering to the fully random disorder case. Indeed, traditional postimplantation doping processes yield in general to a random distribution of dopant atoms. Long-range correlations can possibly break such a complete random character of the disorder. Above a given threshold long-range correlations can even change dramatically the transport properties such as the cancellation of localization effects [6]. Besides postimplantation techniques, the recent bottom-up chemistry approach indicates interesting routes towards the self-assembly of precursors used as building blocks for the fabrication of carbon nanotubes (CNTs) [7–11]. The controlled position of substitutional atoms in precursor monomers can possibly yield in a near future the realization of quasiordered nitrogen-doped CNTs, as already demonstrated for graphene nanoribbons [12,13]. Another source of semi-random disorder can be achieved with the wrapping of DNA strands around the CNT creating disorder with helical symmetry [14,15]. Therefore, with such a large spectrum of disorder, it is expected that localization phenomena emerging from quantum interferences in the diffusion process occur at different paces with various possible intermediate (transient) transport regimes.

In the present theoretical study, subtleties in this rich set of transient transport regimes are analyzed by considering different configurations of nitrogen (N) -doped CNTs, notably the recently proposed semi-random disorder cases [16]. Transport regimes are examined using a real-space Kubo-Greenwood transport approach implemented within the tight-binding (TB) framework [17–19]. This approach enables one to consider system length at the mesoscopic scale (1 μm) and low defect concentration (∼0.1%), further to a recent work [16].

In Sec. II, the tight-binding model and the real-space Kubo-Greenwood approach are briefly reviewed. The following sections discuss the electronic and transport properties of the various configurations of nitrogen-doped armchair CNT. First the perfect CNT, the fully random, and the periodic N-doping configurations are considered as reference structures (Sec. III). Then, intermediate degrees of randomness are taken into account through a particular axial disorder in Sec. IV and helical configurations in Sec. V. Finally, the conclusions are drawn, summarizing the various transport regimes observed in all these configurations of N-doped CNTs including the spectacular ballistic regime obtained for semi-random disorder configurations preserving a rotational symmetry.

II. COMPUTATIONAL METHODS

A. Effective tight-binding Hamiltonian

The CNT wave functions are expanded in a basis set of localized and orthogonal atomic orbitals. In this tight-binding framework, the Hamiltonian matrix elements are parametrized such that the electronic band structure reproduces the *ab initio* results. In the present study, a single π orbital per atomic site is used with first nearest-neighbors interaction hopping parameter set to −2.72 eV. The N impurity potential is considered as a perturbation of on-site terms on the N atom and on the C atoms up to the critical distance $d_{cr} = 7.5$ Å [20–22]. The on-site parameter is taken as zero otherwise to align the Fermi energy of the perfect CNT to zero. The minimal distance between two consecutive N atoms (d_{N-N}) is always kept greater than twice d_{cr} such that the overlap of individual N impurity potentials is avoided. (See Refs. [16,23,24] for details regarding the TB parametrization.)

B. Kubo-Greenwood transport approach: Ballistic, diffusive, and localized regimes

The real-space Kubo-Greenwood transport approach [17–20,25,26], used throughout the present study, focuses on the evaluation of the electronic diffusivity (D) from which the transport regimes can be identified as ballistic, diffusive, or

localized. The diffusivity is computed for each energy E as function of the time t. $D(E,t)$ gives an insight on the diffusion process occurring at different time scale. At short time, or equivalently at short propagation distances, the transport is ballistic and $D(t)$ increases linearly with time, the slope being the square of the average carrier velocity $\langle v^2 \rangle$. At an intermediate time scale (intermediate propagation distances), the diffusivity usually undergoes a sublinear regime because of the first scattering processes with defect impurities. Later, i.e., when enough random scattering processes occurred, the propagation reaches a (thermodynamical) steady state, also called the diffusive regime. In this regime the diffusivity saturates to a maximal value $[D(t) \to D_{\max}]$. At (infinitely) long time, the diffusivity either stays in the diffusive regime or decreases to zero $[D(t) \to 0]$ if localization phenomena occur. According to the scaling theory of localization [2,5], all states are localized in the disordered 1D system; hence diffusivity should always drop to zero at long time. If the system is periodic, i.e., ordered, the diffusivity behavior at infinitely long time is the ballistic regime, which means $D(t) \to \infty$ with a linear increase.

III. PERFECT CNT, PERIODICALLY, AND RANDOMLY N-DOPED CNTS

We consider here perfect, periodically, and randomly N-doped (10,10) CNTs as a model system for metallic CNTs. The unit cell of an armchair (10,10) CNT is composed of 40 atoms which can be sliced along the tube axis into two carbon layers with a tenfold rotational symmetry [top panel in Fig. 1(a)]. In order to ensure a constant concentration of nitrogen, we consider supercells of n_{cell} (10,10) unit cells with one N atom per supercell. Following the long-range symmetry effects found in Ref. [16] we restrict ourselves to n_{cell} equal to a multiple of 3. Consequently, we choose $n_{\mathrm{cell}} = 24$ inducing a concentration of chemical dopants of $\sim 0.1\%$. Since the perfect and the periodically N-doped CNTs are both periodic structures, the Bloch theorem can be applied and hence the band structures of these two systems can be examined [Fig. 1(b) and Fig. 1(c), respectively]. In the random N-doping case, only the density of states (DOS) is accessible. It is computed using the Haydock recursion method [27] applied to a sufficiently long disordered CNT (the system length is $L_{\mathrm{sys}} = 160 d_{\mathrm{sc}} = 945$ nm). The DOS of the three systems are depicted in Fig. 1(d). In Fig. 1(b), the band structure of the perfect (10,10) CNT is simply folded back into the reduced Brillouin zone (BZ) by the artificial supercell translational symmetry. In Fig. 1(c), this band structure is perturbed by the substitution of one N for a C atom. The periodic arrangement of the N dopants introduces a defect band (in the energy window [0.56,0.59] eV) because of the breaking of the original unit cell translational symmetry of the perfect structure (although a translational symmetry exists at the scale of the supercell). Consequently, pseudogaps appear at $\Gamma(k=0)$ and $X(k=\pi/d_{\mathrm{sc}})$, providing splitting effect on the band structure of the perfect system and the loss of transmission channels near the Fermi energy E_F and around the defect energy (E_d) associated to the defect band [16,24]. These pseudogaps correspond to the plateau dips appearing in the DOS indicated by arrows in Fig. 1(d) (black curve). Moreover, when a random
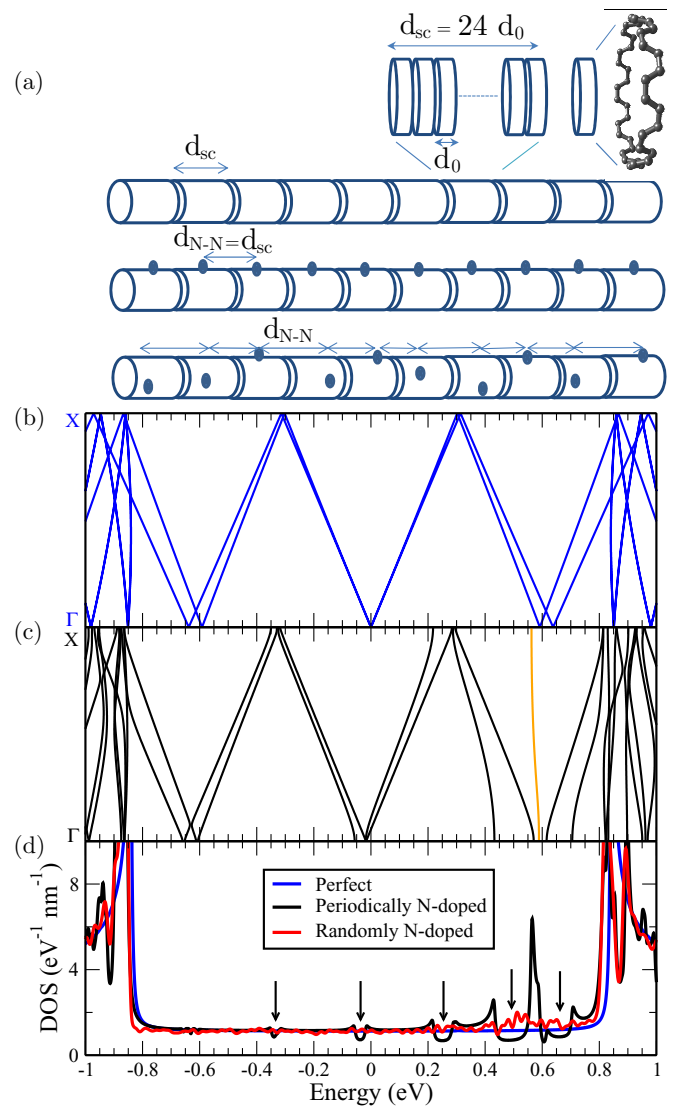

FIG. 1. (Color online) (a) Schematic representation of perfect, periodically, and randomly N-doped armchair (10,10) CNTs. The structure is subdivided into one-atom doped supercells. The length of the supercell (d_{sc}) is determined from the number of unit cells n_{cell} such as $d_{\mathrm{sc}} = n_{\mathrm{cell}} d_0$, d_0 being the CNT's unit cell length. The unit cell is composed of 40 C atoms arranged in two layers. L_{sys} is the system total length. The band structures computed from the tight-binding Hamiltonian for (b) the perfect and (c) the one-N doped supercell ($d_{\mathrm{sc}} = 24 d_0$). The defect band (in orange) is located around the defect energy $E_d \in [0.56, 0.59]$ eV. (d) DOS for the perfect (blue), the periodically N-doped (black), and the randomly N-doped (red) CNT. The DOS of the perfect and periodically N-doped systems are obtained directly from the diagonalization of the TB Hamiltonian, while the DOS of the randomly N-doped system is obtained using the Haydock recursion method ($L_{\mathrm{sys}} \sim 1\ \mu$m).

distribution of the N atoms is considered, the pseudogaps completely disappear in the corresponding DOS. However, allowed minibands seem to be still present around E_d (small bump in the DOS), and splitting on the van Hove singularities is maintained at higher energies, i.e., around $E \sim \pm 0.9$ eV.

The square modulus of the electronic wave functions of the perfect and the periodically N-doped systems at the Γ
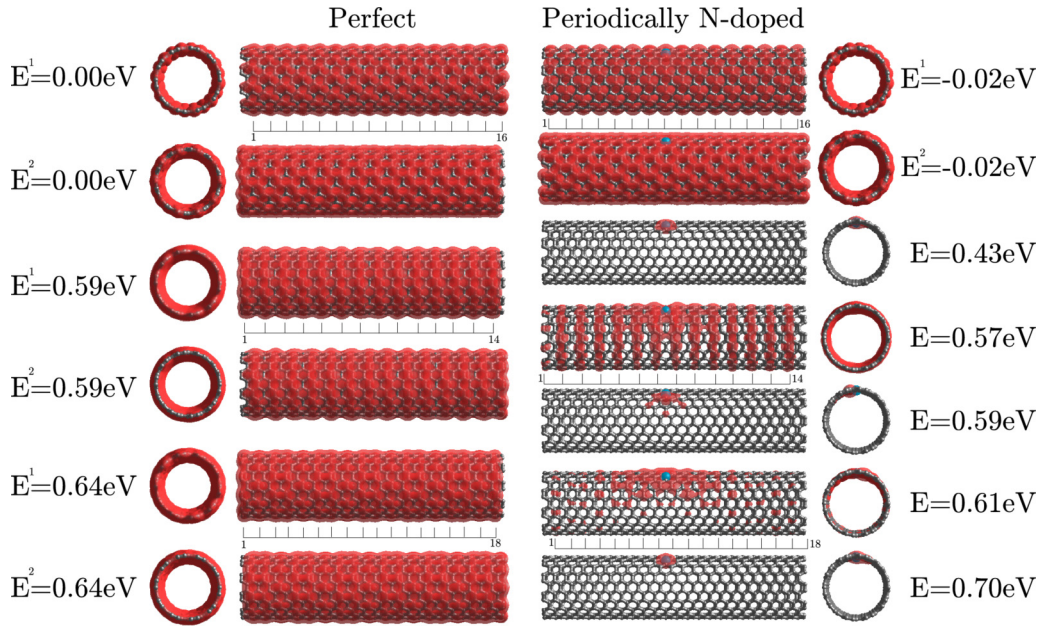
FIG. 2. (Color online) Square modulus of the eigenfunctions of the perfect and periodically N-doped CNTs, at the Γ point and for different energies. All the eigenfunctions of the perfect CNT are extended states, while eigenfunctions of the periodically N-doped CNT are either strongly or slightly localized states around the defect energy (E_d) but still extended states elsewhere. A ruler is given as a guide for the eyes to ease comparison between periodic patterns observed in the perfect CNT and the reminiscent periodic patterns observed for the slightly localized states in the N-doped CNT.

point ($k = 0$) are illustrated in Fig. 2 for energies from $E = 0$ eV to E_d. For perfect tubes, the Γ point in the folded BZ is associated with $k_n = \pm \frac{2n\pi}{24d_0}$ (where d_0 is the unit cell length), and the degenerated bands at $E = 0$ eV correspond to the Dirac points, $n = n_0 = 8$ (i.e., $k_n = \pm \frac{2\pi}{3d_0}$). The next points in Γ are at $E = 0.59$ eV and $E = 0.64$ eV which correspond to $n = n_0 - 1$ and $n = n_0 + 1$, respectively. The two (degenerated) wave functions at $E^{(1,2)} = 0.59$ eV present a periodic annular pattern along the tube. The corresponding period, which in Fig. 2 appears to be $\frac{d_{sc}}{14} = \frac{24d_0}{14}$, is given by half of $\lambda_n = \frac{2\pi}{k_n} = \frac{24d_0}{n}$ (with $n = 7$ for $E^{(1,2)} = 0.59$ eV) since this is the square modulus of the wave function which is plotted. A ruler illustrating the maxima of the square modulus of the wave function is given in Fig. 2 as a guide for the eyes. The next wave functions ($E^{(1,2)} = 0.64$ eV) present also a periodic annular pattern with however an additional tenfold rotational symmetry and a longitudinal period of $\frac{d_{sc}}{18}$ (corresponding to $\lambda_{n=9}/2$). In the case of the periodically N-doped system, while wave functions are almost unaltered close to the zero energy, strongly localized resonant states (also called quasibound states [23,28]) are observed at energies $E = 0.43$, 0.59, and 0.70 eV. The latter correspond to pseudogap band edge states, i.e., bands that largely deviate from the original ones. However, for the bands that deviate less from the perfect CNT, a less localized state is observed which conserves the symmetry pattern of the original wave function of the perfect CNT ($E = 0.57$ eV and $E = 0.61$ eV). More precisely, for $E = 0.57$ eV, the wave function exhibits a similar annular pattern with the same period described above for the perfect CNT ($\lambda_{n=7}/2$), and, for $E = 0.61$ eV, the wave function exhibits a tenfold rotational symmetry with a longitudinal period corresponding to the pristine CNT wave function ($\lambda_{n=9}/2$).

The real-space Kubo-Greenwood approach is now used to examine diffusion processes in the three systems, i.e., perfect, periodically N-doped, and randomly N-doped CNTs. In particular, the nature of the propagating modes around the defect energy E_d is scrutinized by following the time dependence of the diffusivity $D(t)$. As already mentioned, in the periodically N-doped case, the appearance of a defect band (orange line in top panel of Fig. 3) creates localized states which give rise to an enhanced DOS as illustrated in Fig. 3 by the two peaks at the energies E_d^1 and E_d^2. The exact energy position of these two peaks depends on the accuracy level of the technique used to compute the DOS. In Fig. 3, the DOS computed from the band structure using a small broadening parameter ($\eta = 1$ meV) (dashed lines), and the DOS computed from the recursion technique (RT) (thick lines) are compared. For a very accurate DOS calculation from the electronic band structure ($\eta = 1$ meV), the DOS peaks are found to be well aligned with the upper and lower bounds of the defect band (i.e., $E_d^1 = 0.562$ eV and $E_d^2 = 0.588$ eV). However, the use of the RT yields a lower level of accuracy and the defect energies are positioned at $E_d^1 = 0.565$ eV and $E_d^2 = 0.583$ eV (indicated by arrows).

These two propagating modes in the perfect CNT, almost indistinguishable in Fig. 4(a) (full and dashed blue curves), exhibit a linear dependency [$D(t) = v_0^2 t$], endorsing the ballistic transport regime (v_0 is the ballistic velocity). However, when a randomly N-doped CNT is considered, the propagating modes around E_d become localized and the corresponding $D(t)$ starts decreasing exponentially [$D(t) = D_{\max} e^{-\alpha(t - t_0)}$] after a short time ($t_0 = 25$ fs) [Fig. 4(a), red curves]. The localization effects for random distribution have been described by Latil *et al.* [20] and discussed a few years later as an experimental evidence of the Anderson localization phenomena at the mesoscopic scale [29–31]. In opposition with the perfect
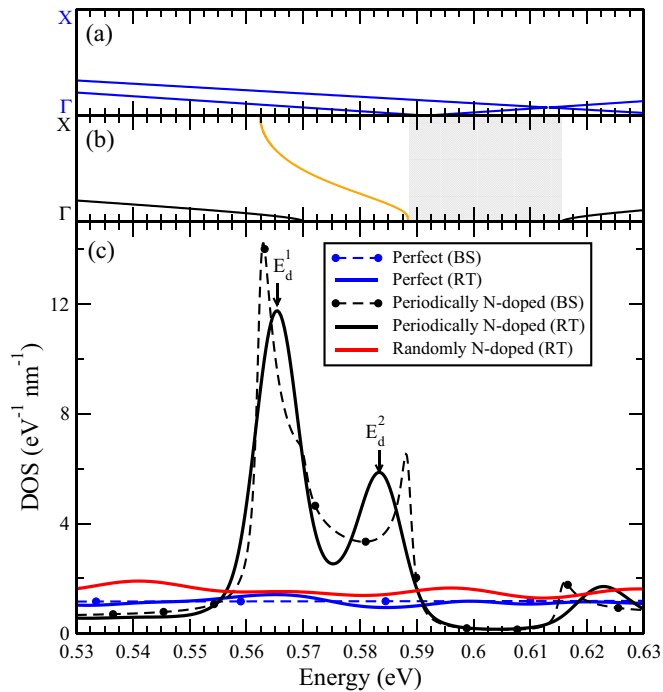
FIG. 3. (Color online) Magnification of the perfect (a) and periodically N-doped (b) CNT band structures around the defect band (orange line). The band gap region in (b) is shaded in gray. (c) The corresponding DOS computed either from the band structures (BS) with a small broadening parameter ($\eta = 1$ meV), or from the recursion technique (RT). Due to limited accuracy of the RT method, the upper and lower bound energies of the defect band (E_d^1 and E_d^2) do not exactly coincide with the BS calculation as indicated by the arrows.
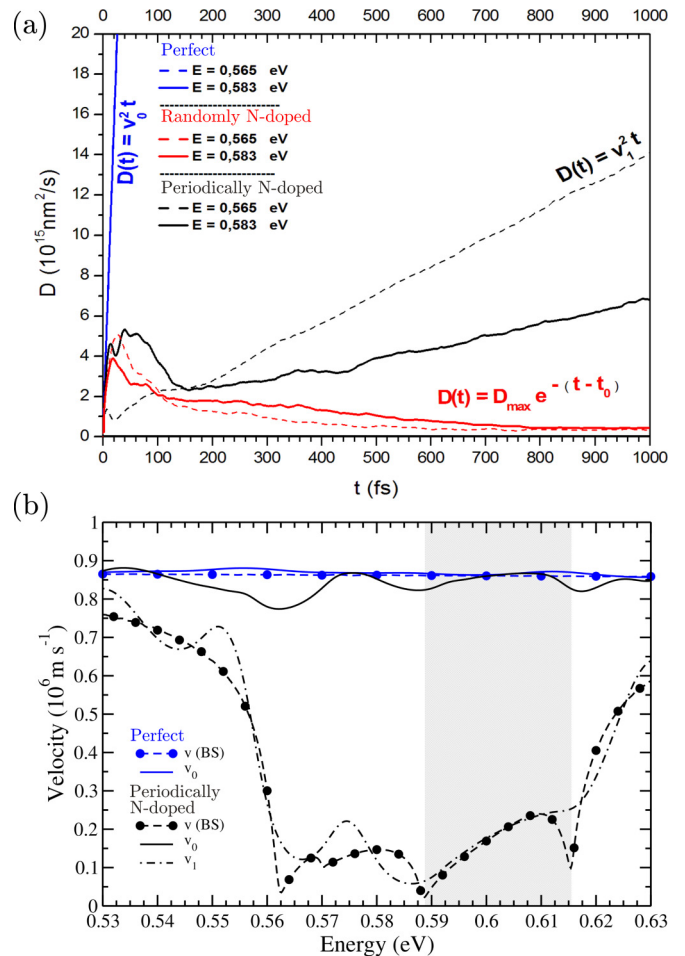

FIG. 4. (Color online) (a) $D(t)$ for the three systems at $E_d^1 = 0.565$ eV and $E_d^2 = 0.583$ eV. (b) Comparison between the velocities of the perfect and periodically N-doped CNTs computed either from the band structures v (BS), or from the Kubo-Greenwood method, i.e., v_0 and v_1 for the short-time and long-time ballistic regimes, respectively. The shaded region corresponds to the gap found in the band structure of the periodically N-doped CNT (see Fig. 3).

and the randomly N-doped structures, the periodic doping scheme presents an interesting sequence of diffusion regimes [Fig. 4(a), black curves], especially at $E = E_d^2 = 0.583$ eV. At short propagation times, $D(t)$ follows the same behavior as for random disorder, i.e., a very short ballistic regime followed immediately by the onset of a localization regime and hence an exponential decrease of $D(t)$. However, this is a transient regime since after a short while ($t > 150$ fs), the diffusion process of the propagating wave packet changes drastically and at longer times, $D(t)$ behaves linearly [$D(t) = v_1^2 t$] meaning that ballisticlike propagating modes are observed. The short- and long-time ballistic velocities, $v_0(E)$ and $v_1(E)$, respectively, are depicted in Fig. 4(b) as a function of the energy for the periodically N-doped structure. At short times, the propagating modes are only slightly perturbed by the defect. In fact, the short-time velocities v_0 of both the periodically N-doped CNT (continuous dark curve) and the perfect CNT are similar (continuous blue curve), and agree well with the average group velocity determined from the band structure, v(BS), of the perfect CNT (blue dashed curve with circle symbols). However, at long times, the propagating modes become more sensitive to the presence of the periodic defect. The ballisticlike velocity v_1 decreases significantly (dark dotted-dashed curve) and the ratio v_1/v_0 gets minimal at the defect energies E_d^1 and E_d^2, i.e., 0.15 and 0.07, respectively. The diffusivity $D(t)$ gives here more information than the band structure, in the sense that before

reaching the long-time ballistic regime, intermediate transport regimes can be captured and two distinct velocities can be calculated. From a propagation point of view, the electrons first experience the perfect CNT on a very short length scale ($\lesssim d_{N-N}$). Then, electrons are progressively scattered by the N atoms but, after a while (~ 3–$4 d_{N-N}$), the periodic arrangement of the N atoms reveals to electrons the ordered nature of the system. Interferences occur and the electrons end up into the supercell Bloch states. At this stage, the ballistic regime is recovered with velocities v_1 corresponding to the group velocities as determined from the supercell band structure [v(BS), dark dashed curve with circle symbols]. One also notes that in the shaded region, which corresponds to the small band gap visible in Fig. 3(b), the values of v_1 are numerically ill-defined because of a nonexactly zero value of the DOS.

IV. AXIAL SEMI-RANDOM CONFIGURATION

In comparison with the previous periodic doping scheme, a constrained randomness of the dopant positions in the
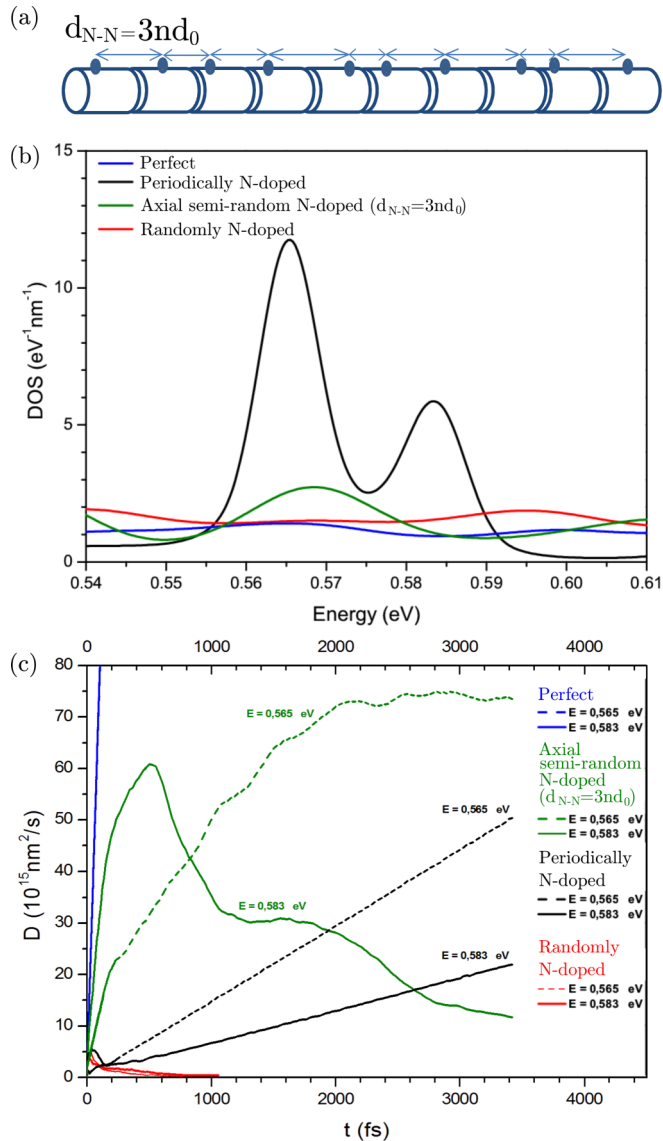
FIG. 5. (Color online) (a) Schematic representation of the axial semirandom configuration. (b) DOS around E_d for the perfect (blue) CNT, and for the periodically N-doped (black), the randomly N-doped (red), and the axial semi-random N-doped ($d_{N-N} = 3nd_0$) (green) CNTs. (c) Long-time behavior of $D(t)$ for the four systems at $E_d^1 = 0.565$ eV and $E_d^2 = 0.583$ eV.

axial direction is considered in this section. The distance between two consecutive N atoms is henceforth restricted to $d_{N-N} = 3nd_0$, where n takes only random integer values [16] [Fig. 5(a)]. The corresponding DOS is presented in Fig. 5(b) (green curve). Compared to the periodic doping configuration (black curve), the DOS no more shows two peaks but presents still a reminiscent peak around $E = 0.57$ eV. In comparison with the cases of the periodically and randomly N-doped configurations studied in Sec. III, the present axial semi-random doping scheme ($d_{N-N} = 3nd_0$) provides peculiar time-dependent behaviors for $D(t)$, recorded here for longer times [green curves in Fig. 5(c)]. Despite the presence of a reasonable amount of randomness, $D(t)$ increases significantly and much faster than in the case of the periodic doping scheme. At the defect energy $E_d^1 = 0.565$ eV, an asymptotic

diffusive regime is observed at long times, without any signs of localization effects (which may appear at even longer time scale). A localized transport regime is however obtained for the propagation mode at E_d^2 but only beyond $t_0 = 500$ fs. This value of t_0, establishing the onset of localization, is considerably larger than for totally random configuration [$t_0 = 25$ fs, Fig. 4(a)]. It is important to emphasize that for a rather long intermediate time scale ($\gtrsim 2$ ps), $D(t)$ is quantitatively higher in this axial semi-random doping scheme than in the periodic doping scheme. However, this is only a transient behavior since in the thermodynamic limit, the electronic diffusion in periodic systems will always exceed the one in semi-random systems because of the linear increase of $D(t)$. Such a crossover is observed at $t \sim 2600$ fs for $E = E_d^2$ in Fig. 5(c). By comparing the fully random disorder case and the present axial semi-random doping scheme, it is obvious that although all states should be localized in disordered 1D systems according to scaling theory, the degree of localization and the rate of its effects on the diffusivity can greatly fluctuate.

V. HELICAL DOPING CONFIGURATIONS

A helical doping configuration is described by a screw operator $S(d,\theta)$. This operator is defined in the polar coordinates (d and θ) by an axial translation d and a rotation with an angle θ that link two successive chemical defects (see Fig. 6) [32]. For the (10,10) CNT, the position of 40 atoms in one unit cell admits a tenfold symmetry ($\theta_0 = 2\pi/10$) and can then be described by four atomic sites (A,B,C,D) [Fig. 6(a)]. For the helical doping configurations considered in this section, d is chosen as a multiple of $3d_0$ as before, and θ as a multiple of θ_0. Therefore, the screw operator $S(d_n = 3nd_0, \theta_m = m\theta_0)$ can be simply noted as $S(n,m)$, n and m being integers. Within this screw operator notation, the doping schemes studied in previous sections are $S(8,0)$ (axial periodic doping), and $S(n,0)$ with random n (axial semi-random doping).

The cases of the ordered and disordered helical doping configurations are now investigated. First, the ordered (periodic) helical configuration is considered with the screw operator $S(8,1)$ [Fig. 6(b)], i.e., $d_{N-N} = 24d_0$ and $\theta = \theta_0$. Then, angular disorder is introduced, keeping the axial ordering, i.e., m equals a random integer [$S(8,m)$, Fig. 6(c)]. Finally, both axial and angular parts are randomized but d and θ are still multiples of $3d_0$ and θ_0, respectively [$S(n,m)$, Fig. 6(d)]. The labeling of all the studied doping configurations using the screw operator notation are summarized in Table I.

The DOS of these three helical doping configurations together with the DOS of the periodic and axial semi-random doping configurations are depicted in Fig. 7(a). Then, $D(t)$ is illustrated in Fig. 7(b) for $E_d^1 = 0.565$ eV and $E_d^2 = 0.583$ eV. The DOS of the $S(8,0)$, $S(8,1)$, and $S(8,m)$ systems are qualitatively indistinguishable and $D(t)$ behave equivalently for these three doping configuration schemes even when m takes random values. Indeed, the long-time ballisticlike permanent regime is spectacularly preserved even in the case of angular disorder although this structure does not possess any periodic arrangement. Furthermore, when the axial periodicity is broken, i.e., when both n and m take random integer values [$S(n,m)$], this particular rotational disorder does not destroy the features obtained for the previous case [$S(n,0)$].
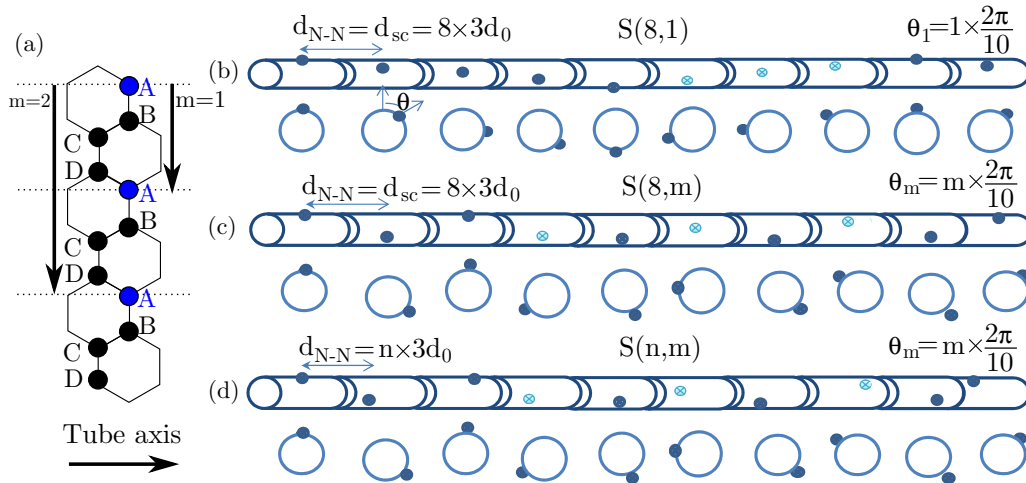
FIG. 6. (Color online) (a) ABCD basis position set in the transversal direction for the (10,10) CNT. Schematic representation for (b) the ordered helical configuration [$S(8,1)$ according to the screw operator $S(d_n,\theta_m) \equiv S(n,m)$ notation], (c) angular disordered helical configuration [$S(8,m)$], and (d) angular and axially disordered helical configuration [$S(n,m)$], n and m being random integers.

The corresponding $D(t)$ shows both diffusive and localized transport regimes [Fig. 7(b)]. This result brings us to the conclusion that the diffusion process is not sensitive to the angular disorder as long as the armchair nanotube rotational symmetry (θ_0) is conserved, i.e., all the N atoms occupy an equivalent position in the basis (A,B,C,D). These results justify the effect of rotational symmetry as recently presented in the electronic transport responses for armchair and chiral nanotubes at shorter length scale [16].

From the present analysis of the diffusion coefficients, it appears clearly that semi-random distributions of the N dopants can yield particularly good transport properties as compared to a random distribution. Indeed, the elastic mean free path of electrons reaches easily several μm for a semi-random configuration like $S(n,0)$ close to Dirac point region ($E = 0$ eV), while it hardly reaches 50 nm for a fully random distribution. Within the defect energy window [0.54–0.61] eV, the mean free paths are lowered and found in the range of [10–700] nm for the semi-random configuration, while it is constant and equal to 5 nm for the fully random case. Consequently, in N-doped CNT with semi-random distribution, the elastic scattering may not be anymore the limiting scattering mechanism and inelastic effects should become important depending on temperature and the applied bias voltage. At low bias, the experimental measurements reported inelastic mean free paths of the order of few μm [33] which correspond

rather well with predicted values for electron scattering with acoustic phonons [33–35]. Elastic and inelastic scattering will therefore compete around $E = 0$ eV; however, close to the defect energy elastic scattering with N dopants should still be more efficient. At high bias, electrons have enough energy to emit optical and zone boundary phonons. The scattering with such phonons gives a much lower inelastic mean free path in the range [10–200] nm [33,36], and hence could become dominant in the present semi-randomly 0.1% N-doped CNTs.

VI. CONCLUSION

The electronic transport regimes in N-doped carbon nanotube has been examined at the mesoscopic length scale using the Kubo-Greenwood formalism and an effective tight-binding approach. The propagating modes in the vicinity of the resonant defect energy have been identified from the time-dependent diffusion coefficient $D(t)$ for various doping configurations, including periodic, semi-random, and random distributions. In all periodic and semi-random doping schemes, the position of dopants is given from the screw operator $S(d_n,\theta_m)$ [$\equiv S(n,m)$] such as $d_n = 3nd_0$ and $\theta_m = m\theta_0$ are the axial and rotational translations, and where $3d_0$ is the Fermi wavelength while $\theta_0 = 2\pi/10$ corresponds to the tenfold rotational symmetry as defined in the (10,10) host CNT. Besides these periodic and semi-random systems, the perfect

TABLE I. (Color online) Labeling and screw operator notation of the different N-doped CNTs.

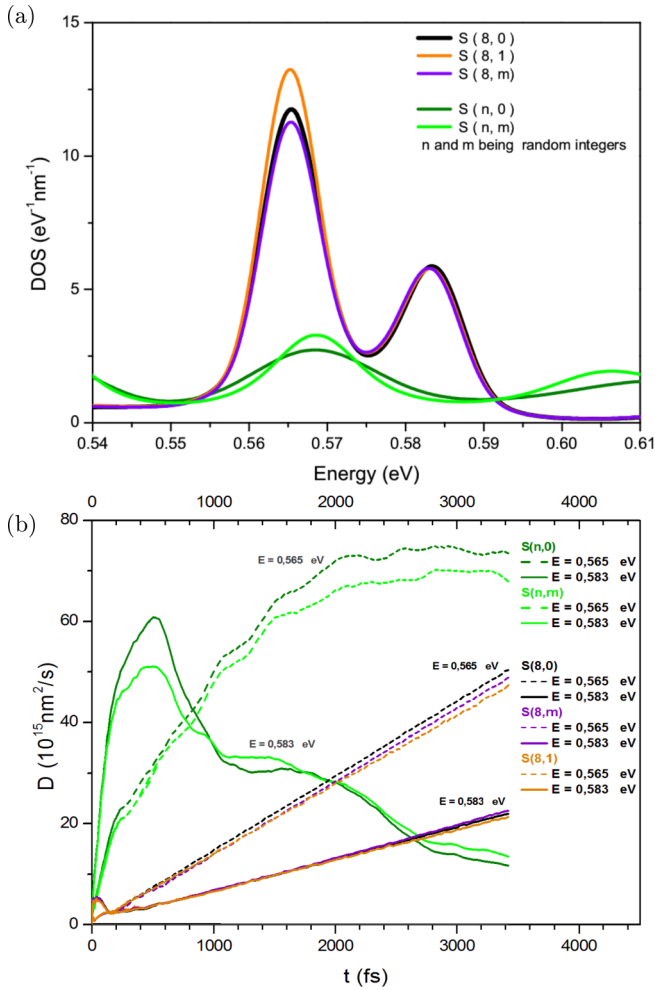| Configuration label	Screw operator	Axial distribution	Angular distribution
Perfect			
Axial periodic	$S(8,0)$	Ordered	
Axial semi-random	$S(n,0)$	Semi-random	
Helical periodic	$S(8,1)$	Ordered	Ordered
Helical angular semi-random	$S(8,m)$	Ordered	Semi-random
Helical semi-random	$S(n,m)$	Semi-random	Semi-random
Random		Random	Random

FIG. 7. (Color online) (a) DOS around E_d different axial and helical doping configurations, i.e., the ordered axial N-doped (black), the ordered helical N-doped (red), the angular disordered helical N-doped (blue), the disordered axial N-doped ($d_{N\text{-}N} = 3nd_0$) (green), and the angular and axial disordered helical N-doped (orange) CNTs. (b) Long-time behavior of $D(t)$ for all these systems at $E_d^1 = 0.565$ eV and $E_d^2 = 0.583$ eV.

CNT and the CNT with a completely random distribution of the N atoms have been considered as reference cases.

For doping configurations with an axial periodicity [e.g., $n = 8$ in $S(n,m)$], ballisticlike transmission modes appear in

the permanent regime [i.e., linear increase of $D(t)$] but with electronic velocities lower than in the perfect CNT and which correspond to the average group velocity determined from the band structure. It is interesting to note that as the tenfold rotational symmetry is kept along the structure [i.e., m can take random integer values], the behavior of the diffusion coefficient $D(t)$ is invariant. Therefore, the semi-random $S(8,m)$ helical doping configuration exhibits also a ballistic regime.

For configurations with a semi-random axial distribution [i.e., $S(n,m)$ with n a random integer], $D(t)$ changes drastically. In these semi-random axial cases, $D(t)$ is found to increase rapidly at the short and intermediate time scale (closer to the ballistic limit of the perfect CNT than the periodic axial configurations), but then saturates (diffusive regime) or even decreases (localization regime) at longer-time scale. Indeed, for the first defect energy (E_d^1), the localization effects seem to be suppressed (or at least shifted to very long time), while quantum interferences leading to localization are well identified for the second defect energy (E_d^2). The rapid increase of $D(t)$ at short-time scales suggests that for short enough CNTs and around the defect energy, such a semi-random axial disorder provides faster electronic diffusion and thus higher conductivities than with a periodic axial configuration. The study of such screw configurations of the disorder are important to understand the implications on the transport properties of the (quasi)periodic helical modifications such as obtained for CNTs wrapped with DNA (DNA-CNTs). These DNA-CNTs are used in particular for the sorting of CNTs in size and chiralities [14,15].

[1] D. J. Thouless, Maximum metallic resistance in thin wires, Phys. Rev. Lett. **39**, 1167 (1977).

[2] P. W. Anderson, D. J. Thouless, E. Abrahams, and D. S. Fisher, New method for a scaling theory of localization, Phys. Rev. B **22**, 3519 (1980).

[3] E. N. Economou and C. M. Soukoulis, Static conductance and scaling theory of localization in one dimension, Phys. Rev. Lett. **46**, 618 (1981).

[4] D. Thouless, Localization in one dimension, in *Physics in One Dimension*, Springer Series in Solid-State Sciences Vol. 23 (Springer, Berlin, 1981), p. 306.

[5] P. A. Lee and T. V. Ramakrishnan, Disordered electronic systems, Rev. Mod. Phys. **57**, 287 (1985).

[6] P. Carpena, P. Bernaola-Galvan, P. C. Ivanov, and H. E. Stanley, Metal-insulator transition in chains with correlated disorder, Nature (London) **418**, 955 (2002).

[7] U. H. F. Bunz, S. Menning, and N. Martn, *para*-Connected cyclophenylenes and hemispherical polyarenes: Building blocks for single-walled carbon nanotubes?, Ang. Chem. Int. Ed. **51**, 7094 (2012).

[8] H. Omachi, Y. Segawa, and K. Itami, Synthesis of cycloparaphenylenes and related carbon nanorings: A step toward the

controlled synthesis of carbon nanotubes, Acc. Chem. Res. **45**, 1378 (2012).

[9] H. Omachi, T. Nakayama, E. Takahashi, Y. Segawa, and K. Itami, Initiation of carbon nanotube growth by welldefined carbon nanorings, Nat. Chem. **5**, 572 (2013).

[10] J. R. Sanchez-Valencia, T. Dienel, O. Groning, I. Shorubalko, A. Mueller, M. Jansen, K. Amsharov, P. Ruffieux, and R. Fasel, Controlled synthesis of single-chirality carbon nanotubes, Nature (London) **512**, 61 (2014).

[11] R. Liu, D. Wu, X. Feng, and K. Mllen, Nitrogen-doped ordered mesoporous graphitic arrays with high electrocatalytic activity for oxygen reduction, Ang. Chem. Int. Ed. **49**, 2565 (2010).

[12] C. Bronner, S. Stremlau, M. Gille, F. Braue, A. Haase, S. Hecht, and P. Tegeder, Aligning the band gap of graphene nanoribbons by monomer doping, Ang. Chem. Int. Ed. **52**, 4422 (2013).

[13] J. Cai, C. A. Pignedoli, L. Talirz, P. Ruffieux, H. Söde, L. Liang, V. Meunier, R. Berger, R. Li, X. Feng, K. Müllen, and R. Fasel, Graphene nanoribbon heterojunctions, Nat. Nanotechnol. **9**, 896 (2014).

[14] M. Zheng, A. Jagota, E. D. Semke, B. A. Diner, R. S. Mclean, S. R. Lustig, R. E. Richardson, and N. G. Tassi, Dna-assisted dispersion and separation of carbon nanotubes, Nat. Mater. **2**, 338 (2003).

[15] X. Tu, S. Manohar, A. Jagota, and M. Zheng, Dna sequence motifs for structure-specific recognition and separation of carbon nanotubes, Nature (London) **460**, 250 (2009).

[16] H. Khalfoun, P. Lambin, and L. Henrard, Long-range resonant effects on electronic transport of nitrogen-doped carbon nanotubes, Phys. Rev. B **89**, 045407 (2014).

[17] D. Mayou, Calculation of the conductivity in the short-mean-free-path regime, EPL (Europhys. Lett.) **6**, 549 (1988).

[18] F. Triozon, S. Roche, A. Rubio, and D. Mayou, Electrical transport in carbon nanotubes: Role of disorder and helical symmetries, Phys. Rev. B **69**, 121410 (2004).

[19] A. Lherbier, S. M.-M. Dubois, X. Declerck, Y.-M. Niquet, S. Roche, and J.-C. Charlier, Transport properties of graphene containing structural defects, Phys. Rev. B **86**, 075402 (2012).

[20] S. Latil, S. Roche, D. Mayou, and J.-C. Charlier, Mesoscopic transport in chemically doped carbon nanotubes, Phys. Rev. Lett. **92**, 256805 (2004).

[21] C. Adessi, S. Roche, and X. Blase, Reduced backscattering in potassium-doped nanotubes: *Ab initio* and semiempirical simulations, Phys. Rev. B **73**, 125414 (2006).

[22] R. Avriller, S. Roche, F. Triozon, X. Blase, and S. Latil, Low-dimensional quantum transport properties of chemically-disordered carbon nanotubes: From weak to strong localization regimes, Mod. Phys. Lett. B **21**, 1955 (2007).

[23] H. Khalfoun, P. Hermet, L. Henrard, and S. Latil, B and n codoping effect on electronic transport in carbon nanotubes, Phys. Rev. B **81**, 193411 (2010).

[24] P. Lambin, H. Amara, F. Ducastelle, and L. Henrard, Long-range interactions between substitutional nitrogen dopants in graphene: Electronic properties calculations, Phys. Rev. B **86**, 045448 (2012).

[25] Z. Fan, A. Uppstu, T. Siro, and A. Harju, Efficient linear-scaling quantum transport calculations on graphics processing units and applications on electron transport in graphene, Comput. Phys. Commun. **185**, 28 (2014).

[26] A. Uppstu, Z. Fan, and A. Harju, Obtaining localization properties efficiently using the kubo-greenwood formalism, Phys. Rev. B **89**, 075420 (2014).

[27] R. Haydock, V. Heine, and M. J. Kelly, Electronic structure based on the local atomic environment for tight-binding bands, J. Phys. C: Solid State Phys. **5**, 2845 (1972).

[28] H. J. Choi, J. Ihm, S. G. Louie, and M. L. Cohen, Defects, quasibound states, and quantum conductance in metallic carbon nanotubes, Phys. Rev. Lett. **84**, 2917 (2000).

[29] C. Gomez-Navarro, P. J. D. Pablo, J. Gomez-Herrero, B. Biel, F. J. Garcia-Vidal, A. Rubio, and F. Flores, Tuning the conductance of single-walled carbon nanotubes by ion irradiation in the anderson localization regime, Nat. Mater. **4**, 534 (2005).

[30] F. Flores, B. Biel, A. Rubio, F. J. Garcia-Vidal, C. Gomez-Navarro, P. de Pablo, and J. Gomez-Herrero, Anderson localization regime in carbon nanotubes: size dependent properties, J. Phys.: Condens. Matter **20**, 304211 (2008).

[31] B. Biel, F. J. Garca-Vidal, A. Rubio, and F. Flores, *Ab initio* study of transport properties in defected carbon nanotubes: an O(N) approach, J. Phys.: Condens. Matter **20**, 294214 (2008).

[32] M. S. Dresselhaus, G. Dresselhaus, and P. C. Eklund, Chapter 19: C60-related tubules and spherules, *Science of Fullerenes and Carbon Nanotubes: Their Properties and Applications* (Academic Press, New York, 1996), Sec. 19.4.

[33] J.-Y. Park, S. Rosenblatt, Y. Yaish, V. Sazonova, H. Üstünel, S. Braig, T. A. Arias, P. W. Brouwer, and P. L. McEuen, Electron–phonon scattering in metallic single-walled carbon nanotubes, Nano Lett. **4**, 517 (2004).

[34] R. A. Jishi, M. S. Dresselhaus, and G. Dresselhaus, Electron-phonon coupling and the electrical conductivity of fullerene nanotubules, Phys. Rev. B **48**, 11385 (1993).

[35] J.-C. Charlier, X. Blase, and S. Roche, Electronic and transport properties of nanotubes, Rev. Mod. Phys. **79**, 677 (2007).

[36] S. Roche, J. Jiang, F. Triozon, and R. Saito, Quantum dephasing in carbon nanotubes due to electron-phonon coupling, Phys. Rev. Lett. **95**, 076803 (2005).